Hanbury Brown and Twiss–Type Experiment with Electrons

William D. Oliver,[1]* Jungsang Kim,[1] Robert C. Liu,[1] Yoshihisa Yamamoto[1,2]

Fermion anti-bunching was directly observed by measuring the cross-covariance of the current fluctuations of partitioned electrons. A quantum point contact was used to inject single-mode electrons into a mesoscopic electron beam splitter device. The beam splitter output currents showed negative cross-covariance, indicating that the electrons arrived individually at the beam splitter and were randomly partitioned into two output channels. As the relative time delay between the outputs was changed, the observed ringing in the cross-covariance was consistent with the bandwidths used to monitor the fluctuations. The result demonstrates a fermion complement to the Hanbury Brown and Twiss experiment for photons.

A thermal boson source tends to emit particles together (bunching) with enhanced particle number fluctuations relative to classical expectations (super-Poisson statistics) (*1*). In contrast, a thermal fermion source tends to emit particles separately (antibunching) with suppressed particle number fluctuations (sub-Poisson statistics) (*2*). Because the statistics are different for bosons and fermions, the covariation of these particles under partition also differs, with the cross-covariation between the two output particle number fluctuations being positive for bosons and negative for fermions (*3*). The positive cross-covariance for photons was demonstrated more than 40 years ago by Hanbury Brown and Twiss (*4*) using photon intensity interferometry, a technique which subsequently became an important tool for probing the statistics of photons generated by various types of sources (*5*). We report the fermion complement to the Hanbury Brown and Twiss experiment, where the negative cross-covariance of partitioned electrons from a single-mode, low-temperature, Fermi-degenerate electron source is demonstrated (*6*).

The partitioning at a beam splitter with transmission probability T of N_1 incident particles in series is a stochastic process, in which the number of particles N_3 transmitted to one output satisfies the probability density, $W(N_3) = \Sigma_{N_1} W_{N_1}(N_3) W(N_1)$, where $W(N_1)$ is the incident particle statistics and

$$W_{N_1}(N_3) = \frac{N_1!}{N_3!(N_1 - N_3)!} T^{N_3}(1 - T)^{N_1 - N_3}$$

is the binomial distribution. This partitioning process introduces fluctuation in the output flux described by the so-called Burgess variance theorem, $\langle \Delta N_3^2 \rangle = \langle \Delta N_1^2 \rangle T^2 + \langle N_1 \rangle T(1 - T)$ (*7*), in which the first term is an (attenuated) input fluctuation and the second term is the partition noise.

The cross-covariance between the two output fluctuations ΔN_2 and ΔN_3 of the beam splitter depends on the fluctuations of the input flux. The normalized cross-covariance (*8*) is defined as

$$\rho(\tau) = \frac{\langle \Delta N_2(t) \Delta N_3(t + \tau) \rangle}{\langle \Delta N_2^2 \rangle^{1/2} \langle \Delta N_3^2 \rangle^{1/2}} \quad (1)$$

where τ is a delay time introduced in the transmitted beam. The close relation between the source fluctuations and the cross-covariance after partitioning is easily demonstrated by considering the case for $\tau = 0$ and $T = 1/2$

$$\rho(\tau = 0) = \frac{F_1 - 1}{\sqrt{F_1 + \frac{1 - T}{T}} \sqrt{F_1 + \frac{T}{1 - T}}} \xrightarrow{T = 1/2} \frac{F_1 - 1}{F_1 + 1} \quad (2)$$

where $F_1 = \langle \Delta N_1^2 \rangle / \langle N_1 \rangle$ is the Fano factor of the source. A source with $F_1 = 1$ emits particles according to the Poisson distribution, where the individual emission events are completely independent of each other, and the resulting cross-covariance of the two outputs after partition is reduced to zero. The cross-covariance of the two output ports is positive for $F_1 > 1$ (super-Poisson input noise) and negative for $0 \leq F_1 < 1$ (sub-Poisson input noise).

In a thermal boson source, stimulated emission results in super-Poisson noise ($F_1 > 1$) giving positive cross-covariance, $\rho(\tau = 0) > 0$, whereas in a thermal fermion source, the Pauli exclusion principle leads to sub-Poisson noise ($0 \leq F_1 < 1$) giving negative cross-covariance, $\rho(\tau = 0) < 0$ (*3*). However, most thermal fermion sources have a very small occupation number per mode, and it is impossible to observe a deviation from the classical Poisson limit. For instance, the best field-emission source of electrons (single-atom nanotip) has an average occupation number per mode of $\sim 10^{-6}$, so the Fano factor is close to the Poisson limit: $F_1 \approx 1 - 10^{-6}$ (*9*).

We fabricated a high-efficiency, single-mode, cold electron source using a high-mobility GaAs two-dimensional electron gas system, which becomes Fermi-degenerate at a cryogenic temperature, and used a quantum point contact to realize a single-mode electron emitter with unity occupation number

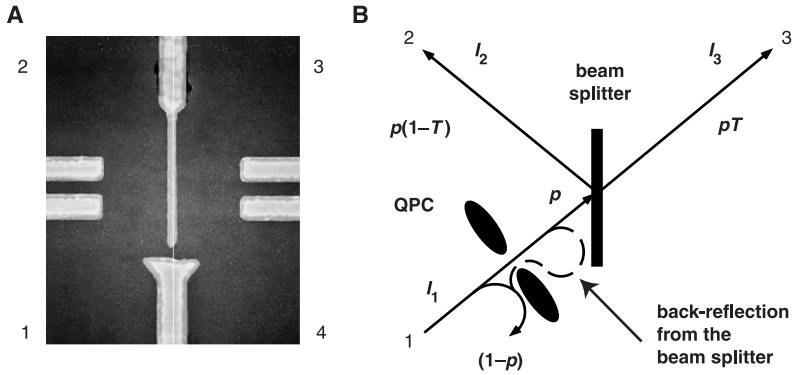

Fig. 1. (**A**) Scanning electron micrograph of an electron beam splitter device fabricated on a GaAs two-dimensional electron gas system. Schottky gates define the input quantum point contact (QPC) (port 1). Schottky gates and an etched trench (top center) define the output QPCs (ports 2 and 3). Port 4 is pinched off. The beam splitter is realized by the 40-nm finger (middle center). (**B**) Transmission and reflection model of the input QPC (port 1) and the beam splitter. I_1 is the input current. I_2 and I_3 are the output currents. The probability p that electrons reach the beam splitter is the normalized conductance of the input QPC (port 1), accounting for the partial transmission through the QPC and the back-reflection from the beam splitter. The beam splitter has a transmission probability T. Prob($1 \rightarrow 3$) = pT. Prob($1 \rightarrow 2$) = $p(1 - T)$.

[1]ERATO (Exploratory Research for Advanced Technology) Quantum Fluctuation Project, Edward L. Ginzton Laboratory, Stanford University, Stanford, CA 94305, USA. [2]Nippon Telegraph and Telephone Basic Research Laboratories, 3-1 Morinosato-Wakamiya Atsugi, Kanagawa, 243-01, Japan.

*To whom correspondence should be addressed. E-mail: woliver@stanford.edu

per mode (*10*). The ballistic and adjustable electron beam splitter was formed monolithically (*11*) by a 40-nm finger, with the splitting ratio tuned by applying a small bias voltage to this finger (Fig. 1A). The inputs (ports 1,4) and outputs (ports 2,3) of the beam splitter are ballistic quantum point contacts defined by a Schottky gate and etched trench (ports 2,3), or by two Schottky gates (ports 1,4), where negative voltage biases applied to the Schottky gates deplete the electrons beneath the gates, controlling the width of the point contacts. The device operates in the ballistic regime, because the length scales for elastic and inelastic scattering at the operating temperature of 1.5 K are much larger than the device size.

The input point contact (port 1) serves as the Fermi-degenerate, single-mode, electron source. The conductance of the point contact is varied by changing the transmission probability p for electrons near the Fermi energy to pass through the constriction (Fig. 1B). The input fluctuations stem from the random scattering of electrons back into the source with a probability of $(1 - p)$. The average current, I, and associated noise spectral density, $S_I(\omega)$, are adjustable via the voltage applied to the Schottky gate of the quantum point contact (*11, 12*)

$$I = G(p)V = \frac{2e^2p}{h}V \quad (3)$$

$$S_I(w) = 2eI(1 - p) \quad (4)$$

Near a gate bias voltage for which the input point contact is pinched off ($p \rightarrow 0$), the conductance approaches zero and the emitted electrons exhibit full shot noise (Poisson limit). As the point contact opens, the conductance increases and the (current-normalized) noise decreases. Once the lowest transverse mode is completely transmitting ($p = 1$), the conductance reaches a plateau, the quantum unit $G_Q = 2e^2/h$, and the noise is completely suppressed (*11, 12*) because the states in the source below the Fermi energy are completely filled and those above the Fermi energy are completely empty.

In the electron cross-covariance experiment, input port 1 is operated as the single-mode electron source, and input port 4 is pinched off. The output ports are biased "open" such that several transverse modes are transmitting, reducing reflections back into the beam splitter. However, the finite reflection of electrons from the beam splitter back toward the input contact reduces the input conductance and creates residual noise (Fig. 1B). Consequently, the experimental input conductance at the plateau is $0.83G_Q$, rather than G_Q. With p used to characterize both the partial transmission through the input point contact and the back-reflection from the beam splitter, and using T to characterize the transmission at the beam splitter with $\bar{T} \equiv (1 - T)$, an analytic expression for the normalized cross-covariance coefficient is given by

$$\rho(\tau = 0) = -\left[\frac{pT \cdot p\bar{T}}{(1 - pT)(1 - p\bar{T})}\right]^{1/2} \quad (5)$$

The output currents I_2 and I_3 from the beam splitter are converted to voltage signals using load resistors, and the ac components are amplified using cascode-configured cryogenic preamplifiers followed by operational amplifiers (*13*). The normalized cross-covariance is then obtained as a function of the delay by the following relation

$$\hat{\rho}(\tau) = \frac{\langle[V_2(t) + V_3(t + \tau)]^2\rangle - \langle[V_2(t) - V_3(t + \tau)]^2\rangle}{\langle[V_2(t) + V_3(t + \tau)]^2\rangle + \langle[V_2(t) - V_3(t + \tau)]^2\rangle}$$

$$= \frac{2\langle V_2(t)V_3(t + \tau)\rangle}{\langle V_2^2\rangle + \langle V_3^2\rangle} \quad (6)$$

where V_2 and V_3 are the voltages corresponding to the output currents I_2 and I_3 and τ is the relative delay between the two outputs. Equation 6 is identical to the cross-covariance (Eq. 1) when $\langle V_2^2\rangle = \langle V_3^2\rangle$. For $p = 1$, this is true for any T. However, for $p < 1$, it is true only for $T = 1/2$; in our experiments, we maintained $T \approx 1/2$. The input currents throughout the experiment typically ranged from 20 to 40 nA, and the noise measurement sensitivity limit in each output branch was 5 nA.

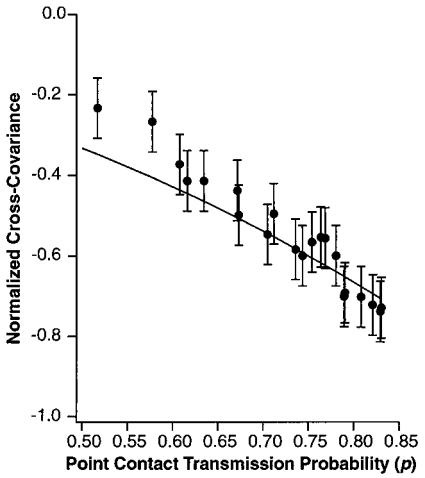

Fig. 2. Experimental normalized cross-covariance with no delay, $\hat{\rho}(\tau = 0)$, as a function of QPC transmission probability p. Because of back-reflection from the beam splitter into the QPC, $p = 0.83$ and $\hat{\rho}(\tau = 0) = -0.73$ at the first conductance plateau in our experiment. As the QPC constriction width is decreased, p decreases from 0.83, and the residual input noise increases. This causes $\hat{\rho}(\tau = 0)$ to decrease in magnitude (approach zero). The solid line is the analytical result based on a probability model accounting for p and T (Eq. 5).

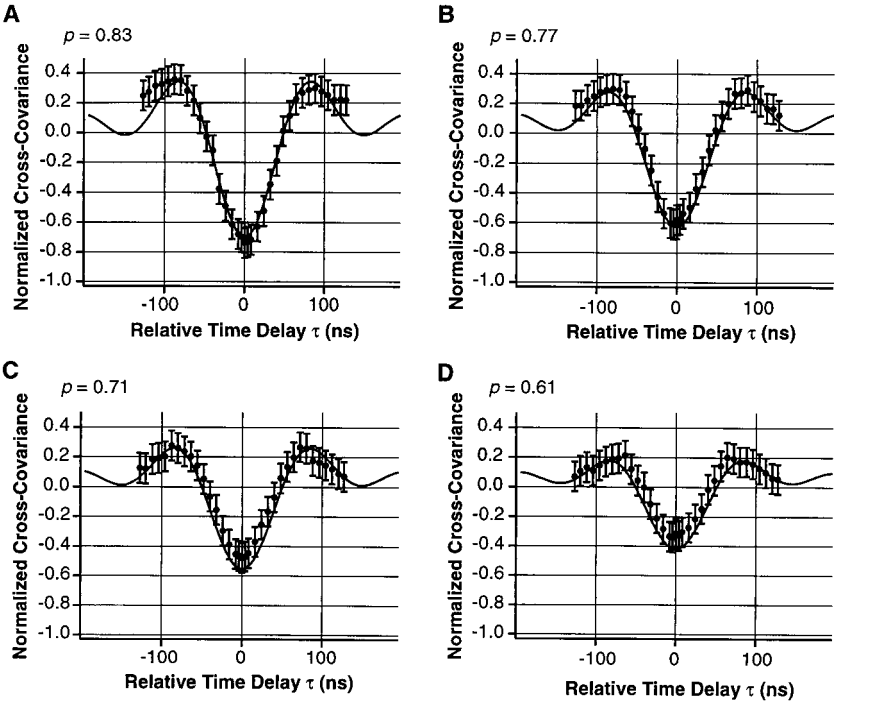

Fig. 3. The normalized cross-covariance is plotted as a function of τ at four values (**A** through **D**) of the input quantum point contact transmission probability: $p = 0.83$, 0.77, 0.71, and 0.61. In each case, the minimum cross-covariance occurs at delay time $\tau = 0$, corresponding to $\hat{\rho}(\tau = 0)$ shown in Fig. 2. The solid line represents the simulated cross-covariance for the actual measurement circuit.

The experimental normalized cross-covariance with no delay, $\hat{\rho}(\tau = 0)$, is plotted against the transmission probability, p, of the input point contact (Fig. 2). As the point contact width is increased, the transmission p through the contact increases and the input electron flux to the beam splitter carries less (current-normalized) noise. The experimental cross-covariance coefficient approaches –1 as p increases, in close agreement with the analytical trace calculated using Eq. 5.

The results are shown for the experimental normalized cross-covariance, $\hat{\rho}(\tau)$, as a function of the delay time at four different conductances, $p = G/G_Q = 0.83$, 0.77, 0.71, and 0.61 (Fig. 3). The values of the experimental cross-covariance at $\tau = 0$ in Fig. 3 are identical to those shown in Fig. 2. As the relative delay between the two output channels is increased, the experimental cross-covariance increases toward zero. The characteristic shape of the experimental cross-covariance data is a direct consequence of the bandpass filter (2 to 10 MHz) used in the measurement circuit (*14*). The additional traces shown are from a numerical simulation which accounts for the point contact transmission p, the beam splitter transmission T, and the entire detection circuit, and closely match the experimental data in all four cases. We emphasize that no fitting parameters have been used in either Fig. 2 or 3 to match the theoretical and simulated traces with the experimental data. Furthermore, the results shown are consistent with the coherent-scattering formalism for calculating current-noise correlations (*15*).

The negative cross-covariance of the output currents of the mesoscopic electron beam splitter directly indicates the sub-Poisson (antibunching) fluctuations of the thermal fermion source. The experimental technique we present is simple and clean. It may prove useful in the measurement of electron current covariance in other mesoscopic systems (*16*), for example, in the study of the statistics of entangled electrons (*17*). One might also use this quantum electron optics technique to probe the source statistics of composite particles in other condensed matter systems, such as the quasi-particles in the fractional quantum Hall regime (*18*), the Cooper pairs in superconductors (*19*), and the excitons in semiconductors (*20*).

References and Notes

1. R. Hanbury Brown and R. Q. Twiss, *Nature* **178**, 1447 (1956).
2. E. M. Purcell, *ibid.*, p. 1449.
3. M. Büttiker, *Phys. Rev. Lett.* **65**, 2901 (1990); *Physica B* **175**, 199 (1991); T. Martin and R. Landauer, *Phys. Rev. B* **45**, 1742 (1992).
4. R. Hanbury Brown and R. Q. Twiss, *Nature* **177**, 27 (1956).
5. G. A. Rebka Jr. and R. V. Pound, *ibid.* **180**, 1035 (1957); H. J. Kimble, M. Dagenais, L. Mandel, *Phys. Rev. Lett.* **39**, 691 (1977); F. Diedrich and H. Walther, *ibid.* **58**, 203 (1987); M. Koashi, K. Kono, T. Hirano, M. Matsuoka, *ibid.* **71**, 1164 (1993); J. Kim, O. Benson, H. Kan, Y. Yamamoto, *Nature* **397**, 500 (1999).
6. M. Henny *et al.* [*Science* **284**, 296 (1999)] have realized independently the Hanbury Brown and Twiss experiment.
7. R. E. Burgess, *Discuss. Faraday Soc.* **28**, 151 (1959).
8. This type of relationship is often referred to as the cross-correlation of two signals. Strictly speaking, the normalized cross-correlation and the normalized cross-covariance are identical only in the case of zero-mean signals. Here, they are identical.
9. M. P. Silverman, *Phys. Lett. A* **120**, 442 (1987).
10. B. J. van Wees *et al.*, *Phys. Rev. Lett.* **60**, 848 (1988); D. A. Wharam *et al.*, *J. Phys. C* **21**, L209 (1988).
11. R. C. Liu, B. Odom, Y. Yamamoto, S. Tarucha, *Nature* **391**, 263 (1998).
12. M. Reznikov, M. Heiblum, H. Shtrikman, D. Mahalu, *Phys. Rev. Lett.* **75**, 3340 (1995); A. Kumar, L. Saminadayar, D. C. Glattli, Y. Jin, B. Etienne, *ibid.* **76**, 2778 (1996).
13. Attenuators were used to match the amplifier gains. Bandpass filters (2 to 10 MHz) eliminated spurious noise at frequencies $f \leq 500$ kHz and matched the high-frequency cutoffs of the amplifiers. Delay lines (0 to 128 ns) were used as necessary for the cross-covariance measurement. The signals were resolved using a hybrid mixer with sum and difference outputs, envelope detectors (square-law devices), and lock-in amplifiers; an ac-modulation scheme was used to improve the signal-to-noise ratio over the thermal noise of the amplifiers. See also (*11, 12*).
14. Ideally, a broad-band measurement circuit would yield a cross-covariance signal containing frequency components from 0 Hz to a high-frequency cutoff of ~100 GHz (the inverse of the electron emission time). Such an ideal cross-covariance signal (plotted versus τ in nanoseconds) would appear to have a very sharp, delta-like anticorrelation at $\tau = 0$ and would quickly go to zero for $\tau \neq 0$. However, cutting off all frequency components higher than 10 MHz creates a sinc-like oscillatory behavior with a center lobe full width at half maximum *FWHM* ≈ 100 ns; this is the inverse of the cutoff frequency 10 MHz. Removing the low-frequency components below 2 MHz introduces a slow dc offset modulation with period ≈ 500 ns, which is manifest in Fig. 3 as an apparent side-lobe dc offset. To the extent that the beam splitter device operates in the linear regime (no frequency mixing), $\hat{\rho}(\tau = 0)$ depends only on the input and beam splitter statistics, regardless of the bandwidth used, because the cross-covariance is normalized by the variances of the filtered stationary signals from the outputs (ports 2 and 3).
15. M. Büttiker, *Phys. Rev. B* **46**, 12458 (1992).
16. Ya. M. Blanter and M. Büttiker, *ibid.* **56**, 2127 (1997); S. A. van Langen and M. Büttiker, *ibid.*, p. 1680; T. Gramespacher and M. Büttiker, *Phys. Rev. Lett.* **81**, 2763 (1998).
17. D. P. DiVincenzo and D. Loss, abstract available at http://xxx.lanl.gov/abs/cond-mat/9901137
18. L. Saminadayar, D. C. Glattli, Y. Jin, B. Etienne, *Phys. Rev. Lett.* **79**, 2526 (1997); R. de-Picciotto *et al.*, *Nature* **389**, 162 (1997).
19. M. J. M. de Jong and C. W. J. Beenakker, *Phys. Rev. B* **49**, 16070 (1994); S. Datta, P. Bagwell, M. P. Anantram, *Phys. Chem. Mater. Low-Dimensional Struct.* **3**, 1 (1996).
20. A. Imamoğlu and R. J. Ram, *Phys. Lett. A* **214**, 193 (1996).

21. We gratefully acknowledge S. Machida for contributions to the cross-correlation circuit and S. Tarucha for contributions to the beam splitter device. W.D.O. gratefully acknowledges continuing support from the National Defense Science and Engineering Graduate Fellowship Program.

7 December 1998; accepted 1 March 1999

The Robust Australopithecine Face: A Morphogenetic Perspective

Melanie A. McCollum

The robust australopithecines were a side branch of human evolution. They share a number of unique craniodental features that suggest their monophyletic origin. However, virtually all of these traits appear to reflect a singular pattern of nasomaxillary modeling derived from their unusual dental proportions. Therefore, recent cladistic analyses have not resolved the phylogenetic history of these early hominids. Efforts to increase cladistic resolution by defining traits at greater levels of anatomical detail have instead introduced substantial phyletic error.

Robust australopithecines are conventionally sorted into three species: a single species from South Africa, *Australopithecus robustus* [1.8 to 1.5 million years ago (Ma)] (*1*), and in East Africa, *A. aethiopicus* (2.7 to 2.3 Ma) and *A. boisei* (2.3 to 1.3 Ma) (*2*). All are characterized by extreme postcanine megadontia, premolars with molarized roots, lower molars with accessory cuspules, and thick molar enamel. All also have sagittal and compound temporal/nuchal extracranial crests, a zygomatic arch positioned high above the occlusal plane, a forward placement of the zygoma, and a robust mandible with an absolutely and relatively tall ramus and a correspondingly tall posterior face (Fig. 1). Robust australopithecines also display markedly small incisors and canines, a thickened hard palate (that part of the upper jaw formed by the palatine process of the maxilla and the horizontal plate of the palatine), a vertically tall infraorbital region, low infraorbital foramina, a face hafted high onto the neurocranium, a frontal region depressed behind the supraorbital torus and between anteriorly converging temporal lines [the frontal trigone (*3*)], and strong postorbital constriction.

Department of Anatomy, Case Western Reserve University, 10900 Euclid Avenue, Cleveland OH 44106, USA. E-mail: mam17@po.cwru.edu